Recovering Reflectance of AQUA MODIS Band 6 Based on Within-Class Local Fitting

Huanfeng Shen, *Member, IEEE*, Chao Zeng, and Liangpei Zhang, *Senior Member, IEEE*

***Abstract*—The Moderate Resolution Imaging Spectroradiometer (MODIS) aboard the Aqua satellite has been working well, except that 14 of the 20 detectors in Aqua MODIS band 6 (1.628–1.652 μm) are ineffective. As a result, the periodic, along-scan strips in Aqua MODIS band 6 create problems in some high-level MODIS products. This paper demonstrates that MODIS bands 6 and 7 are highly correlated for each scene type. On this premise, we propose a within-class local fitting algorithm to recover missing reflectances of Aqua MODIS band 6. To test the efficacy of the proposed algorithm, experiments on real and simulated data are performed and the recovered images are evaluated qualitatively and quantitatively. The experimental results demonstrate that the proposed algorithm performs well.**

***Index Terms*—Aqua, MODIS band 6, recovering, within-class local fitting.**

I. Introduction

THE Moderate Resolution Imaging Spectroradiometer (MODIS) aboard the Terra/Aqua satellite is a major instrument of the NASA Earth Observing System (EOS) [1]–[3]. It has 36 spectral bands ranging from the visible (0.415 μm) to infrared (14.235 μm) spectrum at nadir spatial resolutions of 250 m (bands 1 and 2), 500 m (bands 3 to 7), and 1 km (bands 8 to 39). Since launched, both Terra and Aqua MODIS have been making continuous, complementary morning and afternoon observations (10:30 am equator-crossing orbit for Terra and 1:30 pm equator-crossing orbit for Aqua). The MODIS remote sensing applications are of interest not only to land, ocean, and atmosphere researchers but also to application, interdisciplinary, and environmental scientists [4].

The Aqua MODIS instrument has been performing well except for band 6 (1.628–1.652 μm) [3]–[5]. Fourteen of the 20 detectors are either noisy or non-functional. Therefore, there are periodic, along-scan strips of missing data over the entire image.

Manuscript received May 04, 2010; revised July 20, 2010; accepted August 09, 2010. Date of publication October 18, 2010; date of current version March 23, 2011. This work was supported in part by the Major State Basic Research Development Program (973) of China under Grant 2009CB723905, and the National Natural Science Foundation under Grants 40801182, 40971220, and 40901189.

H. Shen is with the Key Laboratory of Geographic Information System of Ministry of Education, School of Resource and Environmental Science, Wuhan University, Wuhan 430079, China (e-mail: shenhf@whu.edu.cn).

C. Zeng is with the Key Laboratory of Digital Mapping and Land Information Application Engineering, State Bureau of Surveying, and School of Resource and Environmental Science, Wuhan University, Wuhan 430079, China (e-mail: zengchaozc@hotmail.com).

L. Zhang is with the State Key Laboratory of Information Engineering in Surveying, Mapping, and Remote Sensing, Wuhan University, Wuhan 430079, China (e-mail: zlp62@public.wh.hb.cn).

Color versions of one or more of the figures in this paper are available online at http://ieeexplore.ieee.org.

Digital Object Identifier 10.1109/JSTARS.2010.2077620

MODIS band 6 is an important band, which has been widely used in many high-level MODIS products, such as the aerosol product (MOD04), snow cover product (MOD06) and cloud-mask product (MOD35) [5]. Consequently, these MODIS products and other related research have to face the risk of degradation if no reasonable replacement for missing band 6 measurements are found. Therefore, it is necessary to develop a recovery algorithm for improving the radiometric quality of MODIS band 6 products to keep the consistency of the observations.

This research demonstrates that the MODIS bands 6 and 7 are highly correlated for each scene type. On this basis, we developed a within-class local fitting (WCLF) algorithm to recover missing band 6 reflectances. An unsupervised classification is first performed to separate various scene types based on a band selection method. With the classification map, a within-class local fitting is performed to recover every single missing pixel in each type. Moreover, a refinement procedure is included in the local fitting process to eliminate the effect of outliers.

This paper is organized as follows. In Section II, previous methods of recovering Aqua MODIS band 6 reflectances are presented. Section III describes the within-class local fitting method. Experimental results and quantitative evaluations are shown in Section IV, and Section V concludes this paper.

II. Previous Methods

To our knowledge, only two recovery algorithms have been developed for Aqua MODIS band 6. Wang *et al.* [4] were the first to advocate that the Aqua MODIS band 6 be recovered by the stable analytical relationship between Terra MODIS bands 6 and 7. Their research is based on the observation that MODIS bands 6 and 7 are highly correlated over snow coverage. For recovering the Aqua MODIS band 6, the calibrated and geo-located Terra MODIS Level 1B radiances are employed. Polynomial regression was used to quantify the relationship between Terra MODIS bands 6 and 7. Reflectances at the top of the atmosphere (TOA) in Terra MODIS bands 6 and 7 were correlated with a correlation coefficient of 0.9821. Linear, quadratic, cubic, and fourth-degree polynomials were fitted to the data of Terra bands 6 and 7. Wang suggested using the following polynomials:

$$R_{B6} = 1.6032{R_{B7}}^3 - 1.9458{R_{B7}}^2 + 1.7948R_{B7} + 0.012396 \quad (1)$$

or

$$R_{B6} = -0.70472 + 1.5369R_{B7} + 0.025409 \quad (2)$$

where R_{B6} and R_{B7} are reflectances at TOA in Terra MODIS bands 6 and 7, respectively. Similar results are obtained using these two polynomials. In [4], Wang *et al.* emphasized that the

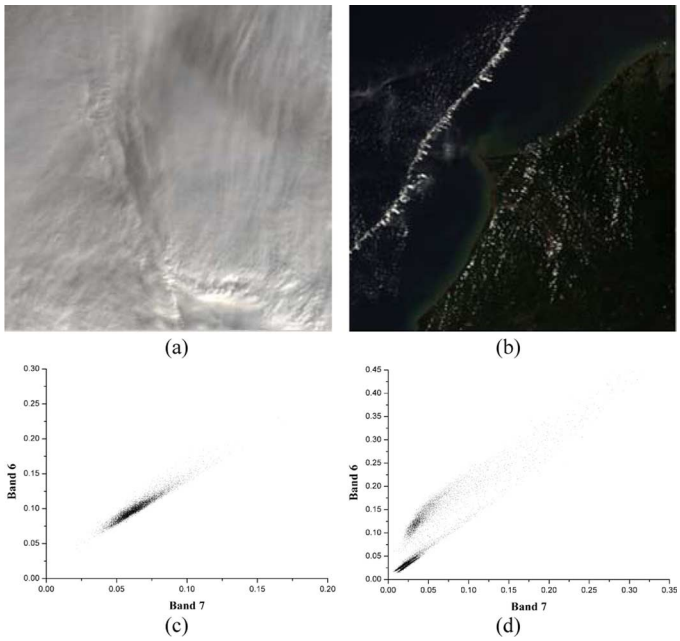

Fig. 1. (a) Sub-image of homogeneous scene, (b) sub-image of heterogeneous scene, (c) scatter plot of (a) using band 6 and band 7 reflectances, and (d) scatter plot of (b) using band 6 and band 7 reflectances.

relationship between these two bands also depends on many factors, such as scene types, spectral characteristics, and scan geometry. Especially the scene type plays a rather important role. As (1) and (2) were developed based on snow cover, their performances are best for snow cover scenes, but have relatively large errors for scenes without snow cover [5].

Rakwatin *et al.* [5] proposed to recover the missing data of Aqua MODIS band 6 by combining a histogram-matching algorithm with local least squares fitting. Histogram matching corrects the detector-to-detector striping of the functional detectors. Local least squares fitting recovers the missing data of the non-functional detectors based on a cubic polynomial derived from the relationship between Aqua MODIS bands 6 and 7. The algorithm was tested on both Terra and Aqua MODIS images, and it can be used on both 1000-m and 500-m pixel resolutions. Using simulated striping images of Terra MODIS data, the results of recovering the synthetic non-functional detectors of band 6 demonstrated that their method can recover the missing data with little distortion. Although this algorithm has greatly improved MODIS band 6 recovery, it also does not consider the effect of scene types.

III. Methodology

A. The Necessity of Classification

As mentioned before, the relationship between Aqua band 6 and 7 reflectances depend on many factors, especially the scene type. To validate this, an experiment has been performed. Fig. 1(a) and (b) show two 1000 by 1000 sub-images of Terra MODIS band 6 and 7 reflectances. One contains homogeneous scene types, and the other contains heterogeneous scene types. Fig. 1(c) and (d) are the scatter plots of band 6 to band 7 reflectance, corresponding to Fig. 1(a) and (b), respectively. From

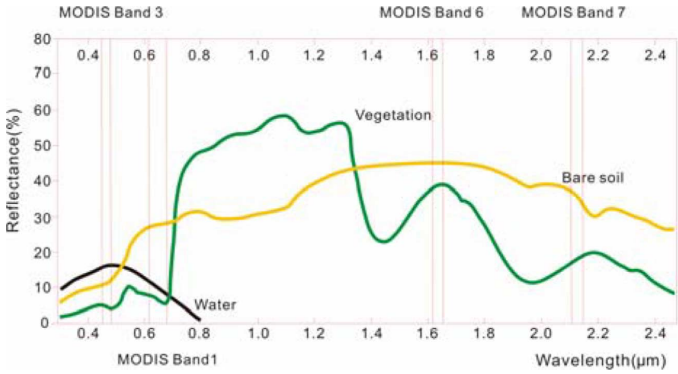

Fig. 2. The reflectance of different scene types in the visible and infrared spectrum.

Fig. 1(c), we can see that bands 6 and 7 are highly correlated when the scene type is homogeneous. However, Fig. 1(d) shows that it is difficult to fit one relation between the two bands using one curve when the image contains different scene types. Therefore, it is necessary to consider the scene types when recovering missing band 6 pixels. To distinguish them, a classification program can be implemented. The two main classification methods are supervised classification and unsupervised classification. In this paper, the unsupervised ISODATA classification method is employed for convenience.

B. Band Selection for Classification

Generally, the bands involved in the classification process should be at the same or an even higher resolution than the recovered band. Since band 6 is at 500-m pixel resolution, the input bands can only be chosen from bands 1 to 7. The purpose of the classification is to separate the various relations between bands 6 and 7 for each scene type. So, the input bands must be as similar to these two bands as possible. If not, the correlation for each scene type will be worse. This situation is especially evident when a scene contains a water body. As Fig. 2 shows, clean water has a much higher electromagnetic wave absorption in the 0.4–2.5 μm range than any other features. With such a low reflectance, water bodies always show a dark appearance in both the visible and near-infrared spectrum. But the reflectance spectrum curves are different for vegetation and soil. They have an absorption close to water in the visible spectrum, while the reflectance becomes much higher than water in the near-infrared range. This means that vegetation and soil or some other features may be as dark as water in the visible spectrum, but also much brighter in the near-infrared spectrum at the same time.

For MODIS, bands 1, 3, and 4 are in the visible spectrum [3]. As Fig. 3(a) shows, the boundary between water and land in the band 1 image is not apparent; a similar situation can also be found in bands 3 and 4. However, Fig. 3(b) shows that in band 7, a water body is much darker than any other feature, which can also be seen in other near-infrared spectrum bands, i.e., bands 2, 5, and 6. Fig. 3(c) is the classification result using visible and near-infrared bands 1, 2, 3, 4, 5, and 7, and Fig. 3(d) is the classification result only using near-infrared bands 2, 5, and 7. Obviously, the selection of only near-infrared bands is more reasonable.

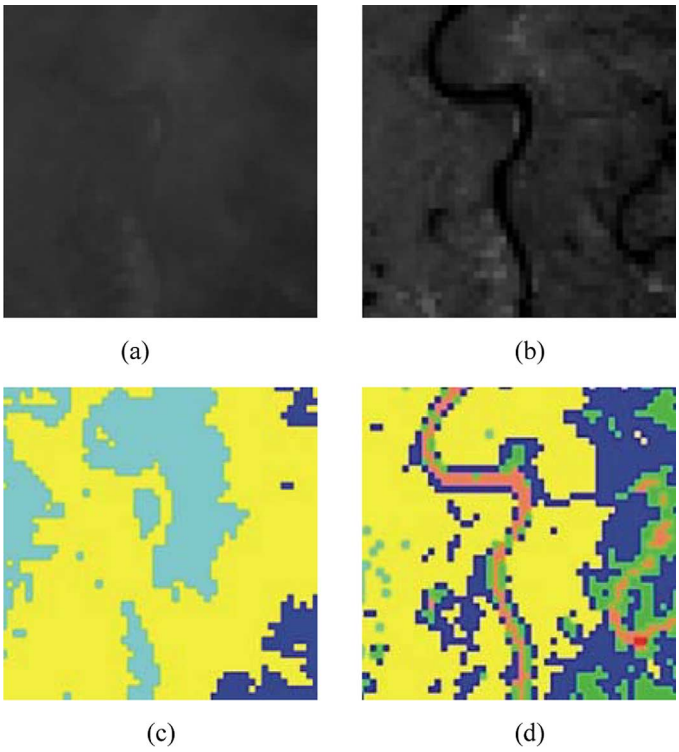

Fig. 3. Sub-images of Aqua MODIS of 500-m pixel resolution acquired on January 16, 2009, over the Yangtze River basin, China. These images are 50 pixels by 50 pixels. (a) Band 1 image, (b) band 7 image, (c) classification result using bands 1, 2, 3, 4, 5, and 7, and (d) classification result using bands 2, 5, and 7.

C. Recovery

To perform data recovery, three images are involved: the band 6 image (P6), the band 7 image (P7), and the unsupervised classification result (Pc) calculated using bands 2, 5, and 7. Generally, it is inadequate to fit a curve using all the pixels from one class. The reasons are as follows. Firstly, according to Tobler's First Law (TFL) [6], near objects are more related, so they are more likely to share similar correlation between bands 6 and 7. What is more, even for the same scene type in an image, the relationship may also depend on some other factors, such as the atmosphere and scan geometry. In general, the relationship is more stable for closer pixels. Therefore, we proposed the following within-class local fitting method.

1) Initialize Fitting Region. For each missing pixel, outline a $N \times N$ rectangular region centered on the missing pixel as the initial region for local fitting.
2) Search for Valid Pixels. Search this region and find the pixels that have a valid value in P6 and belong to the same class in the classification image Pc as the center pixel. These pixels are the nearest valid pixels with a scene type similar to the center pixel. If the number of these pixels is less than a threshold M, enlarge the window until this condition is met. This ensures that sufficient pixels are involved in the curve fitting.
3) Eliminate Outliers. Find the maximum and minimum values in P7 of these valid pixels. If the value of the center pixel in P7 is not between them, enlarge the window until this condition is met. We assume that if the value in P7 of the center pixel is bounded within the search region, the recovered value will be reasonable. This constraint is used to ensure that the result is not an outlier.
4) Curve Fit. Solve for the quadratic polynomial function using the least squares polynomial fitting method with the valid pixels in the fitting region. The following quadratic polynomial function is employed:

$$R_{B6} = aR_{B7}^2 + bR_{B7} + c \tag{3}$$

where R_{B7} is the value of band 7, R_{B6} is the recovered value of band 6, and a, b, and c are the polynomial coefficients. The relations of all valid pixels can be denoted using a matrix-vector form:

$$\mathbf{A} = \mathbf{BX} \tag{4}$$

where $\mathbf{A}$ and $\mathbf{X}$ are vectors containing the values of R_{B6} and polynomial coefficients, respectively, and $\mathbf{B}$ is the corresponding model matrix. Using the least squares method, the coefficients $\mathbf{X}$ can be solved by

$$\mathbf{X} = (\mathbf{B^T B})^{-1}\mathbf{B^T A}. \tag{5}$$

5) Refinement Procedure. In most cases, step 3) works well for outlier elimination and the fitting result of step 4) is satisfactory. However, a very small number of outliers may still appear in some complicated regions. The reason is that in a few cases the maximum or the minimum value is too far away from the others, which leads to a unrealistic fitting error, as shown in Fig. 4(a). To solve this problem, we propose a refinement procedure. The valid pixels in the current window region are checked to determine if there exists at least one pixel whose value in P7 is less than the center pixel satisfy the condition that its distance to the curve is less than a threshold N. And analogously, at least one pixel whose value in P7 is greater than the center pixel in P7 should also satisfy the same condition. If this condition is not satisfied, the window is enlarged and processing returns to step 4) to fit the curve again. In this way, more pixels (hollow circle dots in Fig. 4(b)) are included and the curve fit is improved.
6) Recovery Calculation. Calculate the recovered value of the center pixel using (3) and the solved polynomial coefficients $\mathbf{X}$.

Using the aforementioned procedure, the missing pixels can be recovered one by one. The processing is terminated when all missing pixels are recovered.

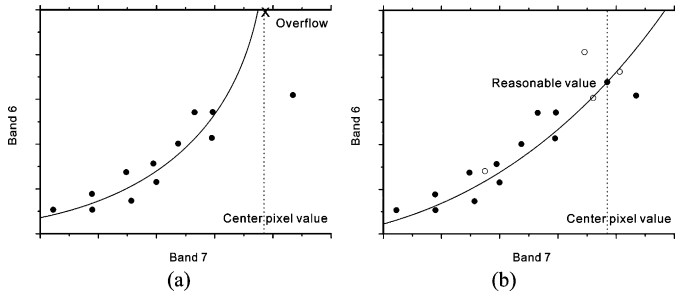

Fig. 4. Illustration of the refinement procedure. (a) Before the procedure, and (b) after the procedure.

IV. Experimental Results

To test the performance of the proposed algorithm, experiments on real Aqua data and simulated Terra data were performed. The data were obtained from the MODIS website of NASA (http://modis.gsfc.nasa.gov/). The 500-m resolution MODIS data used in the experiments are stored as 32-byte floating values, in the standard hierarchical data HDF-EOS format. Information of non-functional and noisy detectors is available in the global attributes of the HDF-EOS metadata. Attributes 48 and 49 are "Dead Detector List" and "Noisy Detector List", which list all the ineffective detectors. It shows that, except for detectors 1, 3, 7, 8, 9, and 11, the other 14 detectors in band 6 are either dead or noisy. Although the missing pixels have been interpolated in the downloaded data, we removed the interpolated values because they are too simply obtained, thereby destroying information and set them to zero for better visual comparison. All data used in the paper are cropped sub-images with 400 pixels by 400 pixels.

To make a comparative analysis, three methods—globe fitting (GF), within-class globe fitting (WCGF), and the proposed within-class local fitting (WCLF)—are implemented. The GF method does not include the classification process, and all the missing pixels are recovered based on the same curve fitted using all the valid pixels in the image. The WCGF method includes classification and global fitting, i.e., the missing pixels belonging to one class are recovered based on the curve fitted using all the within-class valid pixels. In the experiments, ISODATA classification is employed as the unsupervised classification method. The algorithm is not very sensitive to the number of classes. A threshold of 10 is recommended as the maximal number of classes for most images. The actual number is determined by the classification algorithm. For WCLF, the initial window size is set to 17 pixels by 17 pixels, the threshold M in step 2) is set to 30 and the threshold (N in step 5) is set to half of the reflectance value of the center pixel.

Fig. 5(a) shows one of the tested Aqua MODIS images (true color composite R = band 1, G = band 4, B = band 3), acquired on January 18, 2009, over southern China. The original black stripes covering the band 6 image are shown in Fig. 5(b). Fig. 5(c) shows that the pixels are classified into five classes. Fig. 5(d)–(f) are the output images recovered by the GF, WCGF, and WCLF methods, respectively. In Fig. 5(d), there are obvious stripes and artifacts. This result proved that when the image contains complex terrain, it is difficult to develop a reasonable relation between the two bands using one curve, and the incorporation of a classification procedure is reasonable. In Fig. 5(e), most of the recovered pixels match well, but a few stripes still remain. The proposed WCLF algorithm performed excellently. To facilitate detailed visual inspection, a homogeneous region cropped from Fig. 5(b), (d), (e), and (f) is shown in Fig. 6(a)–(d).

Another experiment was performed on an Aqua MODIS image acquired on January 16, 2009, over North Korea. The original image and image resulting from the proposed algorithm are shown in Fig. 7(a) and (b). Fig. 7(c) shows the downloaded image produced using interpolation based method by the MODIS team. Obviously, this image loses much detailed information.

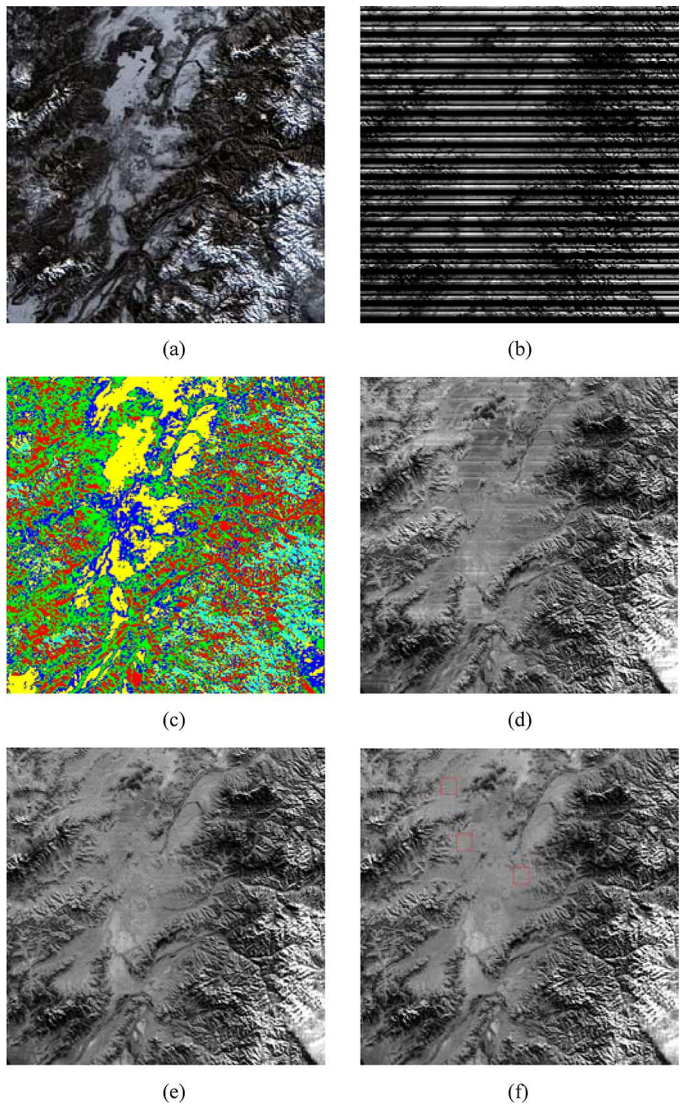

Fig. 5. Sub-images of Aqua MODIS of 500-m pixel resolution acquired on January 18, 2009, over southern China. (a) True color composite R = band 1, G = band 4, B = band 3, (b) original band 6, (c) the classification result calculated by bands 2, 5, 7, (d) recovered by GF method, (e) recovered by WCGF method, and (f) recovered by WCLF method.

The results are quantitatively evaluated using the index of inverse coefficient of variation (ICV) [7]–[9]. In general, ICV values are calculated on homogeneous areas within the image. It can be calculated as follows:

$$\mathrm{ICV} = \frac{R_a}{R_{\mathrm{sd}}} \tag{6}$$

where R_a refers to the signal response of a homogeneous surface and is calculated by averaging the pixels within the window and R_{sd} refers to the noise components estimated by calculating the standard deviation of the pixels within the window. In the experiments, three 20 pixels by 20 pixels homogeneous regions were selected for evaluation in each image, as shown in Figs. 5(f) and 7(b). The evaluation results are shown in Table I. From the ICV perspective, the proposed WCLF algorithm greatly outperforms the GF and WCGF algorithms.

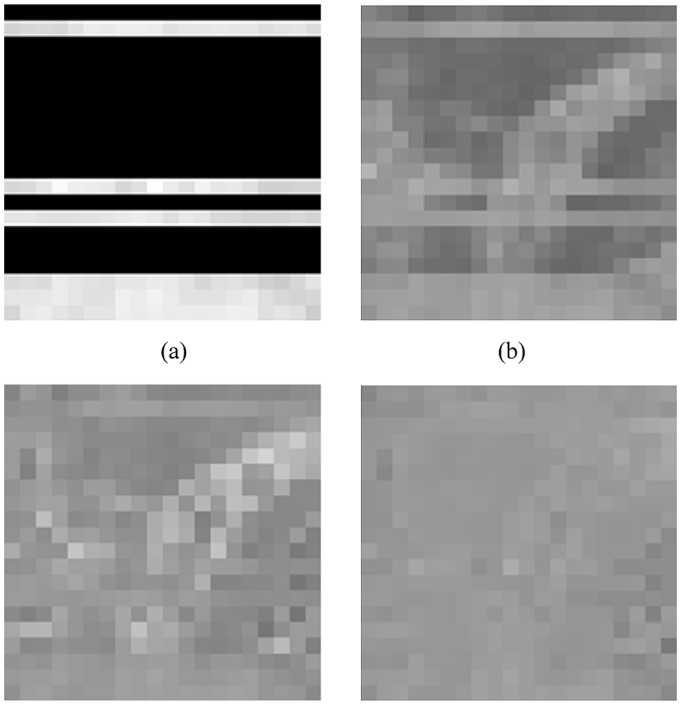

Fig. 6. (a)–(d) Detailed homogeneous regions cropped from Fig. 5(b), (d), (e), and (f).

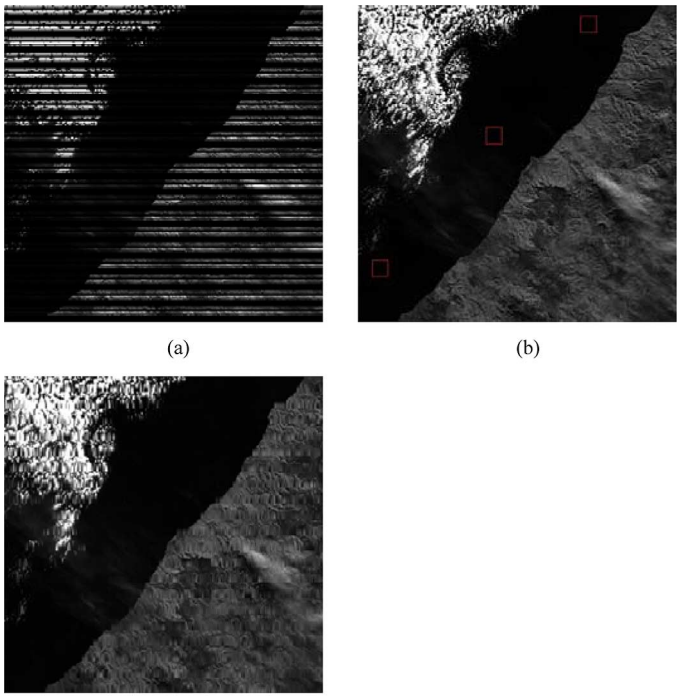

Fig. 7. Sub-images of Aqua MODIS of 500-m pixel resolution acquired on January 16, 2009, over North Korea. These images are 400 pixels by 400 pixels. (a) The original band 6 image, (b) the recovered band 6 image using the proposed WCLF method, and (c) the downloaded image produced using interpolation based method.

The ratio of noise reduction (NR) method [5], [8]–[11] is used to evaluate the recovered image in the frequency domain. It is defined by

$$\mathrm{NR} = \frac{N_0}{N_1} \tag{7}$$

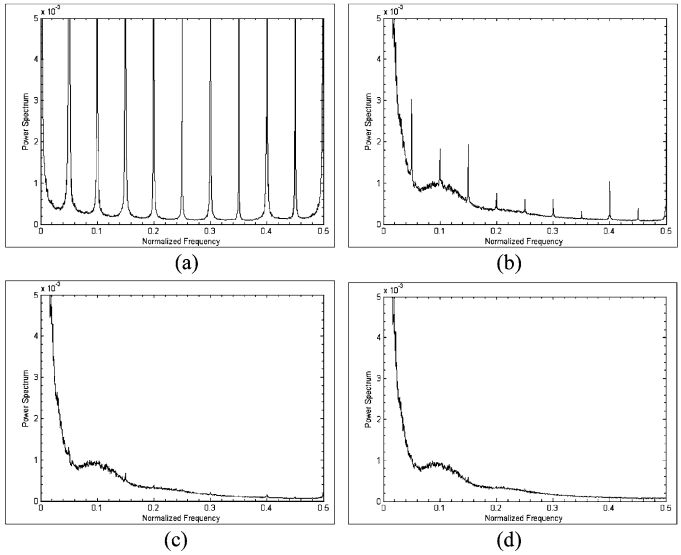

Fig. 8. Mean column power spectrum of the whole Aqua MODIS band 6 image (2708 pixels by 4060 pixels) acquired on January 18, 2009. (a) The original image, (b) recovered by the GF method, (c) recovered by the WCGF method, and (d) recovered by the WCLF method.

where N_0 is the power of the frequency components produced by stripes in the original image and N_1 for the destriped image. N_0 and N_1 can be calculated by

$$N_i = \sum_{\wp} P_i(D) \tag{8}$$

where $P_i(D)$ is the averaged power spectrum down the columns of an image with D being the distance from the origin in Fourier space. Let $\wp$ represent the stripe noise region of the spectrum. For 500-m pixel resolution data, $D \in \{0.05, 0.1, 0.15, 0.2, 0.25, 0.3, 0.35, 0.4, 0.45, 0.5\}$. Table II shows the NR values obtained from the whole image (2708 pixels by 4060 pixels) of Aqua MODIS acquired on January 18, 2009. The proposed algorithm obtains the best evaluation result. Fig. 8 shows the Fourier transforms of the original and recovered data of different algorithms. The horizontal axis represents the normalized frequency, and the vertical axis represents the averaged power spectrum of all columns. In Fig. 8(b), the stripes are still obviously reflected in the frequency domain. Fig. 8(c) shows a better scene, but Fig. 8(d) reveals an even smoother result. The corresponding NR values are shown in Table II.

To further test the performance of the proposed algorithm, Terra MODIS band 6 values have been recovered and compared to the original Terra MODIS band 6 values. The Terra data were acquired on August 1, 2009, over Indonesia, as shown in Fig. 9(a). Fig. 9(b) is the simulated data, and Fig. 9(c) is the classification map. Fig. 9(d)–(f) are, respectively, the recovered images using the GF, WCGF, and WCLF methods. Fig. 10 shows the reflectances for an image column that crosses an area consisting of cloud, sea, and land, which is shown in Fig. 9(a). Note that the proposed algorithm recovers the missing data with very little distortion, even when the scene type changes abruptly.

TABLE I
ICVSOF THE ORIGINAL AND RECOVERED AQUA MODIS DATA

Date	Area	Image	R_a	R_{sd}	ICV
January 18, 2009	Sample 1	Original	0.9666	0.014794	0.653380
		GF	0.029528	0.002931	10.073928
		WCGF	0.032175	0.002156	14.922445
		WCLF	0.032297	0.000972	33.241780
	Sample 2	Original	0.009657	0.014793	0.652825
		GF	0.027634	0.003427	8.064681
		WCGF	0.030918	0.002008	15.397637
		WCLF	0.032303	0.001225	26.378241
	Sample 3	Original	0.009906	0.015167	0.653126
		GF	0.029117	0.002970	9.804125
		WCGF	0.031966	0.001674	19.095314
		WCLF	0.032756	0.001247	26.268924
January 16, 2009	Sample 1	Original	0.000538	0.000829	0.648818
		GF	0.003558	0.001192	2.984936
		WCGF	0.001814	0.000287	6.328817
		WCLF	0.001783	0.000109	16.292551
	Sample 2	Original	0.000733	0.001135	0.645594
		GF	0.004301	0.001272	3.381200
		WCGF	0.003624	0.001573	2.304666
		WCLF	0.002411	0.000267	9.044716
	Sample 3	Original	0.000701	0.001090	0.642913
		GF	0.004145	0.001260	3.289966
		WCGF	0.002400	0.000428	5.605559
		WCLF	0.002438	0.000371	6.578472

TABLE II
NOISE REDUCTION RATIOS OF THE ORIGINAL AND RECOVERED AQUA MODIS DATA

	Original	GF	WCGF	WCLF
NR	1	156	1094	1539

TABLE III
CORRELATION COEFFICIENT, MEAN SQUARE ERROR (MSE), AND AVERAGE RELATIVE ERROR (ARE) OF THE GF, THE WCGF, AND THE PROPOSED WCLF OUTPUT IMAGES

	CC	MSE	ARE
GF	0.932841	0.000706	28.92%
WCGF	0.992660	0.000080	5.21%
WCLF	0.993040	0.000076	4.39%
Idea Value	1.000000	0.000000	0.00%

Fig. 11 shows the scatter plots between the original Terra MODIS band 6 reflectances and the recovered band 6 reflectance. Ideally, all the points should be spread over the 45 degree line. Compared to Fig. 11(a) and (b), (c) shows the closest agreement. Moreover, we can recognize that the points in Fig. 11(a) and (b) are obviously scattered into two main parts, while the points are spread over a continuous range in Fig. 11(c). This is because the region mainly contains sea and land. Fig. 11(a) shows that the error would be unacceptable using the global fitting method. In Fig. 11(b), the reflectances of the recovered data are discontinuous, which means that the WCGF cannot recover the transitional pixels very well. Fig. 11(c) shows that the WCLF can cope with this problem much better.

The correlation coefficient (CC), mean square error (MSE), and average relative error (ARE) between the original Terra band 6 and the recovered band 6 reflectances (shown in Fig. 9) are listed in Table III. The proposed method shows satisfactory results. It should be noted that the Terra MODIS bands 5 and 7 were contaminated by obvious stripe noise, which does not appear in Aqua MODIS bands 5 and 7, so the actual accuracy would be even better.

V. CONCLUSION

This paper presents a method to recover Aqua MODIS band 6 reflectances using within-class local fitting. Compared to previous algorithms, the proposed method incorporates scene types

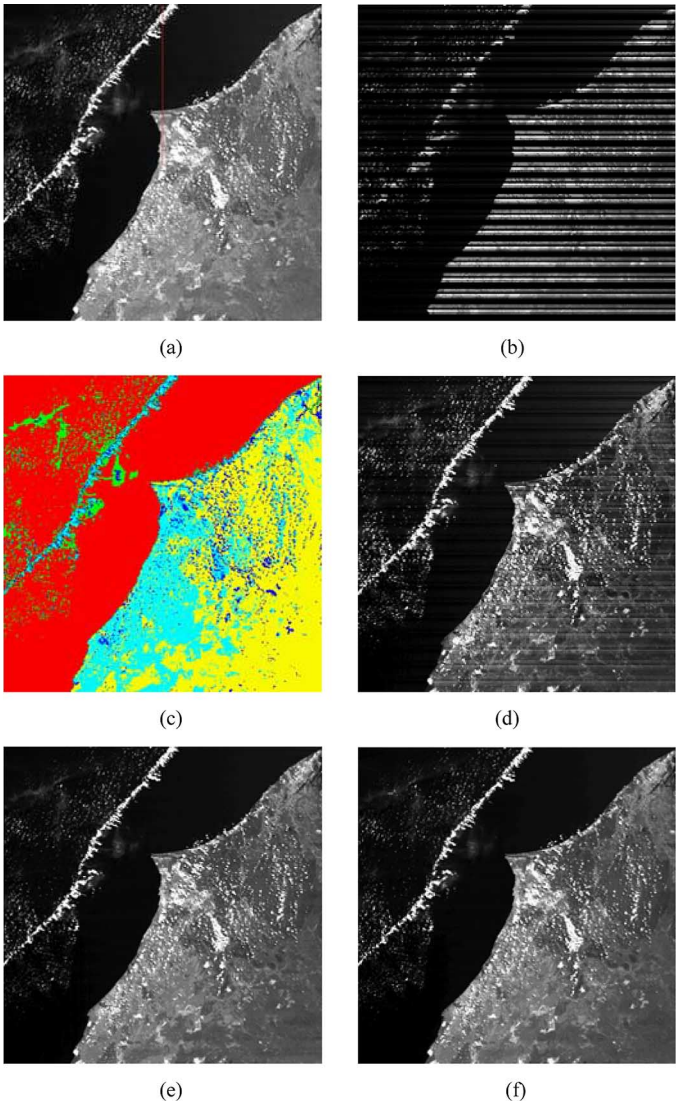

Fig. 9. Sub-images of Terra MODIS of 500-m pixel resolution acquired on August 1, 2009, over Indonesia. These images are 400 pixels by 400 pixels. (a) Original band 6 image, (b) simulated Terra MODIS band 6, (c) the classification result calculated by bands 2, 5, and 7, (d) the band 6 image recovered by the GF method, (e) recovered by the WCGF method, and (f) recovered by the WCLF method.

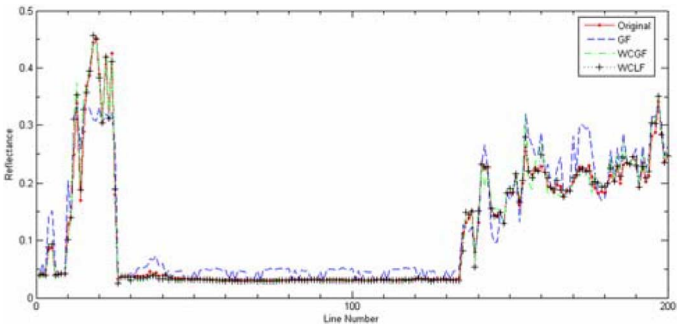

Fig. 10. Reflectances for the image column shown in Fig. 9(a), (d), (e) and (f).

and band spectral characteristics. The method has been tested using both real and simulated data. Some indices, such as the

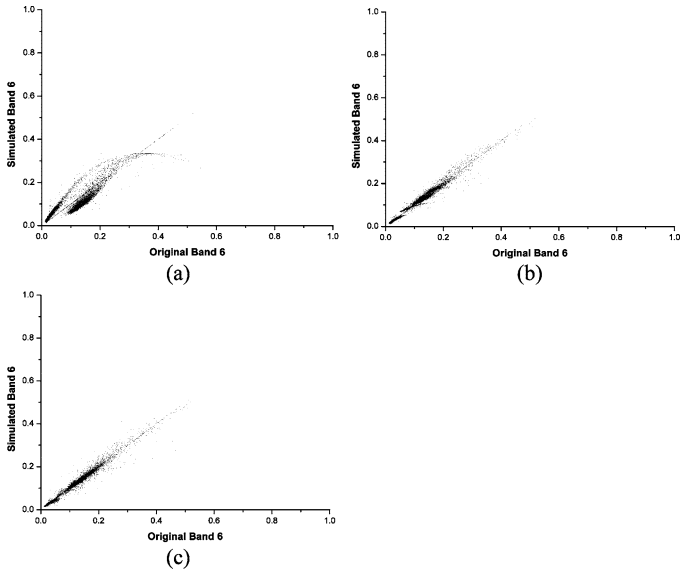

Fig. 11. Scatter plots between the original and recovered Terra MODIS band 6 reflectance data shown in Fig. 8. (a) GF method, (b) WCGF method, and (c) the proposed WCLF method.

inverse coefficient of variation, ratio of noise reduction, correlation coefficient, mean square error and average relative error, are employed for quantitative evaluation. All the experimental results demonstrate that the proposed recovery algorithm performs well. Further work can potentially expand the method to incorporate a fast implemention strategy.

REFERENCES

[1] A. Savtchenko, D. Ouzounov, S. Ahmad, J. Acker, G. Leptoukh, J. Koziana, and D. Nickless, "Terra and Aqua MODIS products available from NASA GES DAAC," *Trace Constituents in the Troposphere and Lower Stratosphere*, vol. 34, pp. 710–714, 2004.

[2] X. Xiong, N. Che, Y. Xie, D. Moyer, W. Barnes, B. Guenther, and V. Salomonson, "Four-years on-orbit spectral characterization results for Aqua MODIS reflective solar bands," in *Sensors, Systems, and Next-Generation Satellites X*, Stockholm, Sweden, Sep. 11–13, 2006, vol. 6361, p. 6361OS-1.

[3] X. Xiong, K. Chiang, J. Sun, W. L. Barnes, B. Guenther, and V. V. Salomonson, "NASA EOS terra and Aqua MODIS on-orbit performance," *Advances in Space Research*, vol. 43, no. 2, pp. 413–422, Feb. 2009.

[4] L. L. Wang, J. J. Qu, X. X. Xiong, X. J. Hao, Y. Xie, and N. Z. Che, "A new method for retrieving band 6 of Aqua MODIS," *IEEE Geosci. Remote Sens. Lett.*, vol. 3, pp. 267–270, Apr. 2006.

[5] P. Rakwatin, W. Takeuchi, and Y. Yasuoka, "Restoration of Aqua MODIS band 6 using histogram matching and local least squares fitting," *IEEE Trans. Geosci. Remote Sens.*, vol. 47, pp. 613–627, Feb. 2009.

[6] W. Tobler, "A computer movie simulating urban growth in the detroit region," *Economic Geography*, vol. 46, pp. 234–240, 1970.

[7] G. Smith and P. Curran, "Methods for estimating image signal-to-noise ratio (SNR)," in *Advances in Remote Sensing and GIS Analysis*, P. M. Atkinson and N. J. Tate, Eds. Hoboken, NJ: Wiley, 2000, pp. 61–74.

[8] P. Rakwatin, W. Takeuchi, and Y. Yasuoka, "Stripe noise reduction in MODIS data by combining histogram matching with facet filter," *IEEE Trans. Geosci. Remote Sens.*, vol. 45, pp. 1844–1856, Jun. 2007.

[9] H. F. Shen and L. P. Zhang, "A MAP-based algorithm for destriping and inpainting of remotely sensed images," *IEEE Trans. Geosci. Remote Sens.*, vol. 47, pp. 1490–1500, May 2009.

[10] J. Chen, Y. Shao, H. Guo, W. Wang, and B. Zhu, "Destriping CMODIS data by power filtering," *IEEE Trans. Geosci. Remote Sens.*, vol. 41, pp. 2119–2124, 2003.

[11] G. O. Young, "Synthetic structure of industrial plastics," in *Plastics*, J. Peters, Ed., 2nd ed. New York: McGraw-Hill, 1964, vol. 3, pp. 15–64.

Huanfeng Shen received the B.S. degree in surveying and mapping engineering and the Ph.D. degree in photogrammetry and remote sensing from Wuhan University, Wuhan, China, in 2002 and 2007, respectively.

In July 2007, he joined the School of Resource and Environmental Science, Wuhan University, where he is currently an Associate Professor. His research interests focus on image reconstruction, remote sensing image processing and application, data fusion and assimilation.

Chao Zeng received the B.S. degree in resources environment and urban planning management from Wuhan University, Wuhan, China, in 2008. He is currently pursuing the Master degree in the School of Resource and Environmental Science, Wuhan University. His current research interests focus on remote sensing image processing.

Liangpei Zhang received the B.S. degree in physics from Hunan Normal University, ChangSha, China, in 1982, the M.S. degree in optics from the Xi'an Institute of Optics and Precision Mechanics of Chinese Academy of Sciences, Xi'an, China, in 1988, and the Ph.D. degree in photogrammetry and remote sensing from Wuhan University, Wuhan, China, in 1998.

From 1997 to 2000, he was a Professor in the School of Land Sciences, Wuhan University. In August 2000, he joined the State Key Laboratory of Information Engineering in Surveying, Mapping and Remote Sensing, Wuhan University, as a Professor and head of the Remote Sensing Section. Since 2007, he has been nominated as a "ChangJiang Scholar" professor (Chair Professor) by the Education Ministry of China. He has published more than 150 research papers. His research interests include hyperspectral remote sensing, high resolution remote sensing, image processing, and artificial intelligence.